



CHORUS

This is the accepted manuscript made available via CHORUS. The article has been published as:

Spectral linewidth of a Ne-like Ar capillary discharge soft-x-ray laser and its dependence on amplification beyond gain saturation

L. Urbanski, M. C. Marconi, L. M. Meng, M. Berrill, O. Guilbaud, A. Klisnick, and J. J. Rocca

Phys. Rev. A **85**, 033837 — Published 29 March 2012

DOI: [10.1103/PhysRevA.85.033837](https://doi.org/10.1103/PhysRevA.85.033837)

Spectral linewidth of a Ne-like Ar capillary discharge soft x-ray laser and its dependence on amplification beyond gain-saturation

L. Urbanski¹, M.C. Marconi¹, L.M. Meng², M. Berrill³, O. Guilbaud⁴,
A. Klisnick², J.J. Rocca¹

1. NSF ERC for Extreme Ultraviolet Science and Technology, Colorado State University, Fort Collins, CO 80523

2. ISMO, Bât. 350, CNRS, Université Paris-Sud 11, Orsay

3. Oak Ridge National Laboratory, Oak Ridge Tennessee 37831

4. LPGP, Bât. 210, CNRS, Université Paris-Sud 11, Orsay

Abstract

We report the measurement of the linewidth and temporal coherence of a $\lambda = 46.9$ nm neon-like argon capillary discharge soft x-ray laser and its variation with plasma column length. A wavefront division interferometer was used to resolve the $3p\ ^1S_0-3s\ ^1P_1$ laser line, resulting in a measured relative linewidths of $\Delta\lambda/\lambda = 3-4 \times 10^{-5}$. The measurements do not observe saturation re-broadening as this clearly dominantly Doppler-broadened inhomogeneous line is amplified beyond the intensity corresponding to gain saturation. Model simulations indicate this is the result of a comparatively small collisional broadening that sufficiently homogenizes the line profile to practically eliminate inhomogeneous saturation re-broadening. Collisional re-distribution is computed to play only a very minor role in homogenizing the line profile.

1. Introduction

Capillary discharge soft x-ray lasers, first demonstrated in 1994 [1], remain to date as the highest average power table-top source of coherent soft x-ray radiation [2,3]. The capillary discharge Ne-like Ar laser operating at $\lambda = 46.9$ nm is also the table-top soft x-ray laser most broadly utilized in applications. It has been used in interferometric studies of high density plasmas [4], high resolution microscopy [5,6], holographic imaging [7], nano-scale patterning and machining [8,9], material ablation [10,11], single-photon ionization mass spectrometry studies of nanoclusters [12], the measurement of optical constants of materials [13], and other applications. This practical table-top laser has been widely characterized. The gain [1,14-16], output pulse energy [2,3,16,17], pulse duration [1,2,16,17], beam divergence [1,2,15-17], and wavefront characteristics [18] have been measured. The spatial coherence of the beam has also been measured to increase as a function of plasma column length [19], reaching essentially full spatial coherence in capillary discharges 36 cm in length [20]. However, the spectral line-width and the temporal coherence, which are important parameters in applications such as interferometry and large area nano-patterning, remained to be characterized.

Besides the practical interest in knowing the temporal coherence of capillary discharge lasers for applications, the measurement of the line-width behavior as a function of plasma column length is also of significant interest for fundamental reasons [21,22]. This is so because this laser media offers the opportunity to study the gain-saturation behavior of a highly inhomogeneous line. In soft x-ray laser amplifiers created by laser irradiation of solid targets the amplified laser lines have not been observed to significantly re-broaden as their intensity increases beyond the saturation intensity [21,22]. This

observed lack of inhomogeneous saturation rebroadening was attributed by Koch et al. to homogenous lifetime-broadening resulting from electron collisions with the radiating ions, and to collisional redistribution effects that can be expected to effectively homogenize the Doppler component [21]. The latter is the result of velocity-changing collisions that transfers populations among the different velocity groups of the radiating ions such that no longer a single velocity is associated with each radiator (collisional redistribution). The capillary discharge plasma amplifiers differ from those laser-pumped solid-target collisional soft x-ray lasers in that the electron density is typically up to two orders of magnitude lower, while the ion temperature exceeds the electron temperature. The Doppler broadening contribution clearly dominates the Voigt line profile and the collisional component that homogenizes the line profile is much less significant. This highly inhomogeneous line profile could be expected to lead to the observation of saturation re-broadening of the line not observed in previous studies of line amplification in soft x-ray plasma amplifiers [21,22]. The relatively low electron density and moderate ion temperature that characterizes the capillary discharge plasma amplifiers also gives origin to a small linewidth that is further narrowed in the amplification process. This results in a very narrow laser line that is difficult to measure because its width is below the resolution of most existing spectrometers at this wavelength. Several measurements of the linewidth of different types of laser-pumped soft x-ray lasers have been reported [22-27]. These measurements were conducted using either a custom-made spectrometer of extremely high resolution [22], or different types of interferometers [23-27].

In this paper we report the first measurements of the linewidth and temporal coherence of a capillary discharge neon-like argon soft x-ray laser, and compare the results to model

simulations. The variation of the line-width as a function of amplifier plasma column length was measured for plasma lengths between 18 cm and 36 cm. The measurements were conducted using a wavefront-division interferometer specifically designed to measure the temporal coherence of soft x-ray sources [27]. The line profile was inferred from the measurements of the fringe visibility as a function of path difference in the interferometer. This interferometer was previously used to investigate other types of collisional soft x-ray lasers, including a 32.8 nm injection-seeded optical-field-ionization soft x-ray lasers in a Xe gas medium [23] and injection-seeded and self-seeded transient collisional soft x-ray lasers in the 18.9 nm line of Ni-like Mo in plasmas created by laser irradiation of solid targets [26].

2. Experimental method

The experimental set up used in the linewidth measurements is shown in Fig. 1. The capillary discharge laser beam is reflected by two 45° incidence angle Sc-Si multilayer mirrors that are used to steer the beam for alignment with the interferometer axis. Due to its limited reflective bandwidth, the set of multilayer mirrors serves as a band-pass filter that eliminates the unwanted background caused by off-band plasma emission. The wave-front division interferometer is based in a pair of dihedrons slightly tilted towards each other and irradiated at 6° grazing incidence (Fig. 1) [27]. This set up splits the incoming beam in two branches that are made to interfere onto the surface of a back-thinned CCD detector. The CCD is located at 50 cm from the bi-mirror and is tilted at an angle of 35 ° relative to the propagation axis to improve the spatial resolution. A precision translation stage vertically displaces one of the bi-mirrors relative to the other

inducing a controlled optical path difference between the two interfering beams. The change in optical path difference introduces a controlled phase shift between the two beams which in turn modifies the contrast of the interference fringes. A more detailed description of the instrument can be found in ref. 27.

Figure 2a shows a typical capillary discharge laser interferogram obtained with the optical path difference set to zero. The overlap of the reflections from the by bi-mirror creates a rectangular interference region of $\sim 1.5 \times 14 \text{ mm}^2$ dimension at the detector. The relative alignment of the two beams determines the orientation and density of the fringes observed. A cross section of the interferogram in Fig. 2b, shows a visibility of 80%, indicating a high degree of spatial coherence. The measurements were conducted for discharges in a 3.2 mm diameter capillary channel filled with a pressure of 440 mTorr of argon excited by a 21 kA peak amplitude current pulse with a 10- 90% rise-time of 44 ns. This current pulse amplitude, the maximum that can be obtained in this set up for a 36 cm long capillary, is smaller than that of some of the previously reported capillary lasers [2,3] but matches that of the most compact capillary discharge lasers [17]. It was selected to allow us to maintain the current pulse amplitude, and hence the plasma conditions, practically constant as the capillary length was increased from 18 cm to 36 cm to study the gain-saturation linewidth behavior. At the discharge conditions of this experiment the far field laser beam pattern was recorded to be characterized by a doughnut shape (inset in Fig. 1) with a peak-to-peak divergence of 3.8 mrad (FWHM divergence of 4.4 mrad), resulting from refraction of the amplified beam in the radial density gradient of the cylindrical plasma column. It is possible to use the refraction

angle measured from the far-field pattern to estimate the maximum electron density [28, 29], in this case $\sim 1.8 \times 10^{18} \text{ cm}^{-3}$.

The spatial coherence of the beam was measured to decrease with decreasing plasma length of the neon-like Ar capillary discharge laser [20]. At the location of our interferometer, 5 m from the capillary exit, the spatial coherence radius can be estimated from these measurements to be of the order of 1 and 4 mm for the 18 cm and 36 cm long capillaries respectively. For the measurements described in this paper, this means that the maximum visibility at the zero path difference is not constant, but monotonically decreases when the plasma length is varied from 36 to 18 cm. Nevertheless it should be understood that the dihedron reflector interferometer design assures that the same two regions of the beam interfere as the path length difference is changed [27]. This makes the measured loss of visibility independent of the variation of the spatial coherence for different capillary lengths, and solely dependent on the temporal coherence.

3. Measurements, simulations and discussion

Figure 3 shows the measured variation of the fringe visibility as a function of optical path difference for a 36 cm long capillary discharge plasma column. Each value results from averaging the visibility measured for five laser shots. The figure also shows raw interferograms corresponding to different path differences, along with a Gaussian fit to the data that yields a temporal coherence length L_c defined as the e^{-1} visibility point in the Gaussian profile of $L_c = 690 \text{ }\mu\text{m}$. The corresponding linewidth is of $16.6 \text{ m}\text{\AA}$, or $\Delta\lambda/\lambda = 3.5 \times 10^{-5}$.

Figure 4a shows the measured variation of the laser output intensity, and Fig. 4b shows the corresponding measured variation of the laser line bandwidth as a function of capillary plasma column length. This graph shows measurements that span plasma column lengths that are shorter and longer than the saturation length, that is observed to occur at $L_s \sim 24$ cm. Figure 4a and b also compare the data to the result of a model simulation that computes the line propagation along the amplifier axis taking into account gain saturation and refraction losses. The model simulates the amplification of the laser line by solving the frequency dependent intensity and population equations accounting for Doppler and collisional broadening, gain saturation, beam refraction, and collisional redistribution. The line transport is computed by breaking the different ion velocities into subgroups, solving the population equation including stimulated emission for each velocity subgroup, and using the natural lineshape with collisional broadening to obtain the frequency dependent gain profile for each subgroup. The subgroups are summed to obtain the total frequency dependent lineshape, which is used to solve the frequency dependent intensity equation. In turn, the total frequency dependent intensity is used to calculate the stimulated emission rate for each population subgroup. The resulting system of equations are coupled together into a combined solver. Refraction losses are estimated according to reference [29] from the doughnut shape far-field beam profile shown in the inset in Fig. 1. Collisional redistribution of the population subgroups is accounted for in a way similar to that described by Koch et al [21] by considering that ion-ion collisions change the ion velocities in the direction of the laser beam, and using the ion-ion collision time to obtain the redistribution rate. This results in an additional term that couples the equations governing the different population subgroups.

The simulation results shown in Fig. 4 correspond to a plasma with an electron density of $1.8 \times 10^{18} \text{ cm}^{-3}$ derived from the beam divergence measured from far-field beam refraction pattern, to ion temperatures of 70 eV, 87 eV and 100 eV, and to the electron temperatures that produces the best fit in each case. The corresponding electron temperatures required to obtain the best fit of the experimental data do not change significantly, ranging from 87.4 to 92.6 eV. The value of the electron temperature required to fit the data also depends on the fraction of neon-like ions, that for the fit in Fig. 4 was assumed to be 0.75. For different fractions of neon-like ions ranging from 0.8 to 0.6 the electron temperature corresponding to the best fit varies from 88.5 eV to 98.1 eV. For the plasma conditions used to obtain the fits in Fig. 4 the Doppler and Lorentzian contributions to the line-profile are computed to be $7.3 \times 10^{11} \text{ Hz}$ and $5.4 \times 10^{10} \text{ Hz}$ respectively. Most of the line narrowing due to amplification is computed to take place at plasma column lengths shorter than 18 cm, the minimum length at which the laser beam intensity was sufficiently high to allow for reliable interferometry measurements. The line does not significantly re-broaden after gain saturation is reached, contrary to the case of a purely inhomogeneously broadened line. The simulations predict only a small amount of re-broadening, that mostly falls within the error bars of the measurements. Instead the line maintains a value of $\Delta\lambda/\lambda \sim 3.5 \times 10^{-5}$. Collisional redistribution, which was previously considered by Koch et al. [21,22] and Pert [30] to affect the amplification dynamics of laser-pumped collisional soft x-ray lasers created by irradiation of solid targets [21,22], is computed to play only a very small role in the saturation behavior of capillary discharge laser. This is illustrated in Fig. 4c that shows small differences between fits to the data that include or neglect the effect of velocity-

changing ion-ion collisions. The fits were performed with collisional re-distribution rates corresponding to either the ion-ion collision time from Lee and Moore [31] (19 ps) or from a molecular dynamics computation performed specifically for the argon ions of interest (27 ps) [32]. The absence of observable re-broadening after gain saturation, caused by homogenization of the line profile by collisional broadening takes place in spite of the fact that capillary discharge lasers operate in a regime in which Doppler broadening greatly dominates the line profile. Since the capillary discharge plasmas have up to two orders of magnitude lower plasma density than those corresponding to laser-pumped collisional soft x-ray lasers that use solid targets [22,24-27], and a higher ion temperatures than that characteristic of optical-field-ionization soft x-ray lasers [33], it is difficult to find among the current soft x-ray lasers plasma conditions in which the inhomogeneous component is more dominant. This suggests that the observation of saturation re-broadening in soft x-ray plasma amplifiers would be an unusual event.

4. Conclusions

In conclusion, we have conducted the first measurement of the linewidth and temporal coherence of a capillary discharge soft x-ray laser, and have studied its variation as a function of amplifier length. While the line profile in this discharge amplifier is clearly dominated by Doppler broadening, the relatively small collisional broadening component is still sufficiently large to homogenize the line to the point at which no re-broadening was measured to take place as the line intensity continued to increase beyond gain saturation. The narrow relative linewidth of this laser, $\Delta\lambda/\lambda = 3-4 \times 10^{-5}$, corresponds to a coherence time of ~ 2 picoseconds that is much shorter than the pulse duration, of 1.2-

1.8 ns [2,3,17]. The degree of temporal coherence of the capillary discharge 46.9 nm laser is thus significantly lower than those previously measured in two other types of collisional SXRLs, namely a 32.8 nm optical-field-ionization SXRL in a Xe gas medium [23], and the 13.9 nm and 18.9 nm transient collisional soft x-ray lasers in Ag and Mo plasmas created by laser irradiation of solid targets [25,26]. The difference arises from the fact that while these laser-pumped systems are transient gain systems in which the laser pulse duration of a few picoseconds is relatively close to full temporal coherence, the capillary discharge laser is essentially a quasi-CW laser in which the laser pulse duration is more than two orders of magnitude longer than both the upper laser level lifetime and the laser pulse of the transient lasers. Nevertheless, the $L_c \sim 700 \mu\text{m}$ (e^{-1}) temporal coherence length measured for this capillary discharge SXRL is either similar or in some cases even larger than that of other collisional soft x-ray lasers [24-26], which facilitates applications requiring high temporal coherence, such as interferometry [4] and large-area Talbot nano-patterning [34].

Acknowledgments

We acknowledge fruitful discussion with A. Calisti (PIIM, Université de Marseille, France) on ionic correlations. The support and expertise from D. Joyeux and S. de Rossi (LCF, Institut d'Optique, Palaiseau, France) are greatly appreciated. This work was supported by NSF Award PHY-1004295, the NSF Center for Extreme Ultraviolet Science and Technology under NSF Award EEC-0310717, DTRA under contract N° HDTRA 1-10-1-0070, and by the AMOS program of the Office of Basic Energy Sciences, U.S. Department of Energy. M. B. acknowledges support for staff members at

Oak Ridge National Laboratory managed by UT-Battelle, LLC, for the U.S. Department of Energy under Contract No. DE-AC05-00OR22725.

Figure Captions

Figure 1: Schematic representation of the experimental set up. The output of the table top EUV capillary laser is aligned with the axis of the bi-mirror interferometer using two multilayer mirrors that also contribute to filter off-band plasma radiation. The wavefront-division interferometer produces two beams that interfere onto a CCD. The inset shows the doughnut-shape of the far field profile of the laser beam recorded using a CCD. The size of the detector did not allow the recording of the entire beam.

Figure 2: a) Typical interferogram corresponding to the zero path length difference in the interferometer. The interferogram corresponds to a capillary discharge plasma column 21 cm in length. . b) Line-out of the interferogram computed from the region within the box. (a).

Figure 3: Visibilities as a function of optical path difference for a capillary discharge plasma column 36 cm in length. The insets are interferograms that illustrate the deterioration of the fringe visibility with increased path difference due to finite temporal coherence. The line is a Gaussian fit to the data.

Figure 4: a) Measured laser output intensity as a function of capillary discharge plasma column length. Gain saturation is observed to occur for a plasma column length of ~ 24 cm. b) Measured laser linewidth as a function of discharge plasma column length. Five independent measurements of the line width were averaged for each capillary length. The error bars were selected to include all measurements. The lines are the results of simulations for the plasma conditions discussed in the text, assuming ion temperatures of

100eV, 87 eV and 70 eV from top to bottom respectively. The computations take into consideration collisional redistribution. c) The lines show the computed variation of the linewidth neglecting (full line) and including (dashed lines) collisional redistribution.. The denser dashed line was computed using the ion-ion collision time of Lee and More and the other using a collision time determined by a molecular dynamics computation [32]. The plasma parameters are those described in the text and the ion temperature is 87 eV.

Figure 1

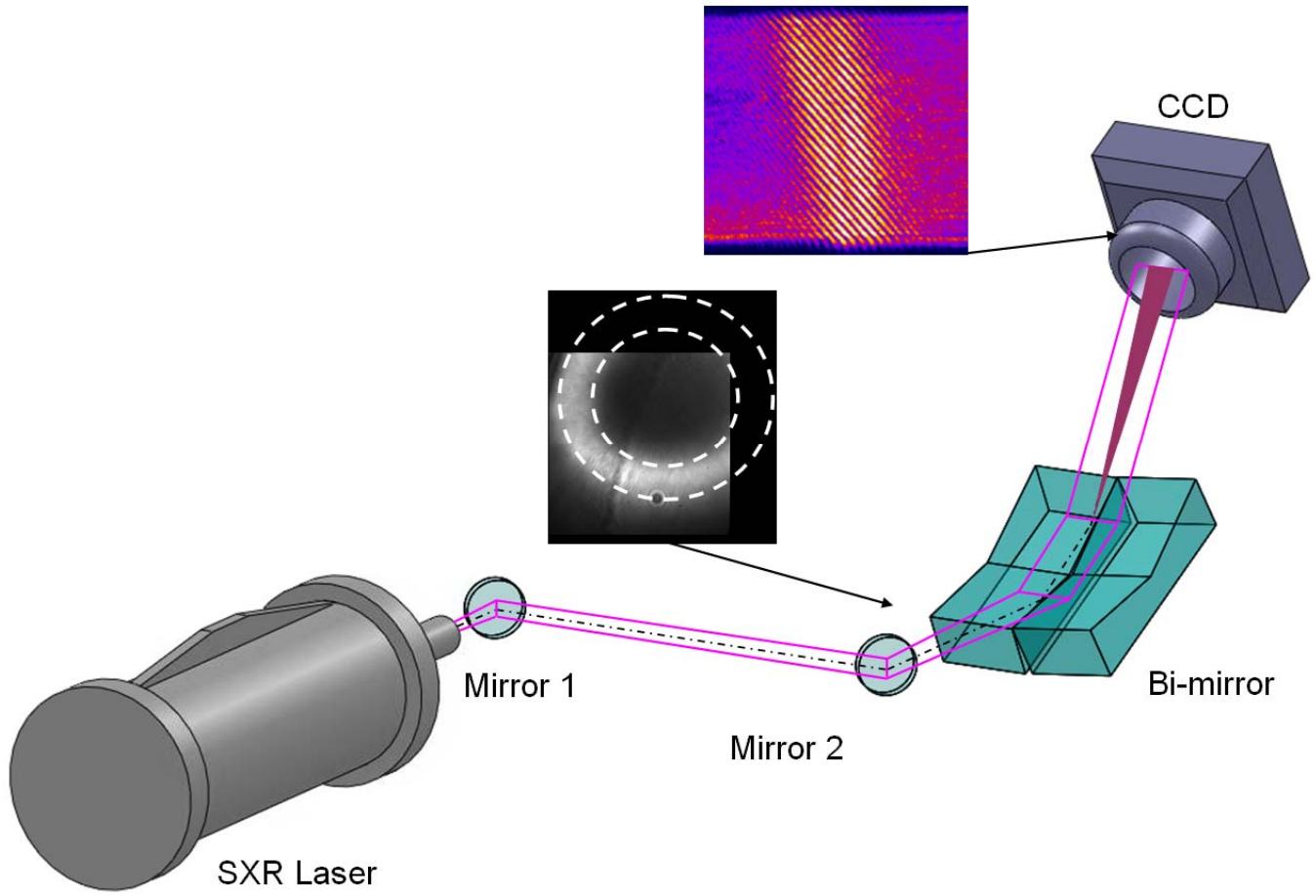


Figure 2

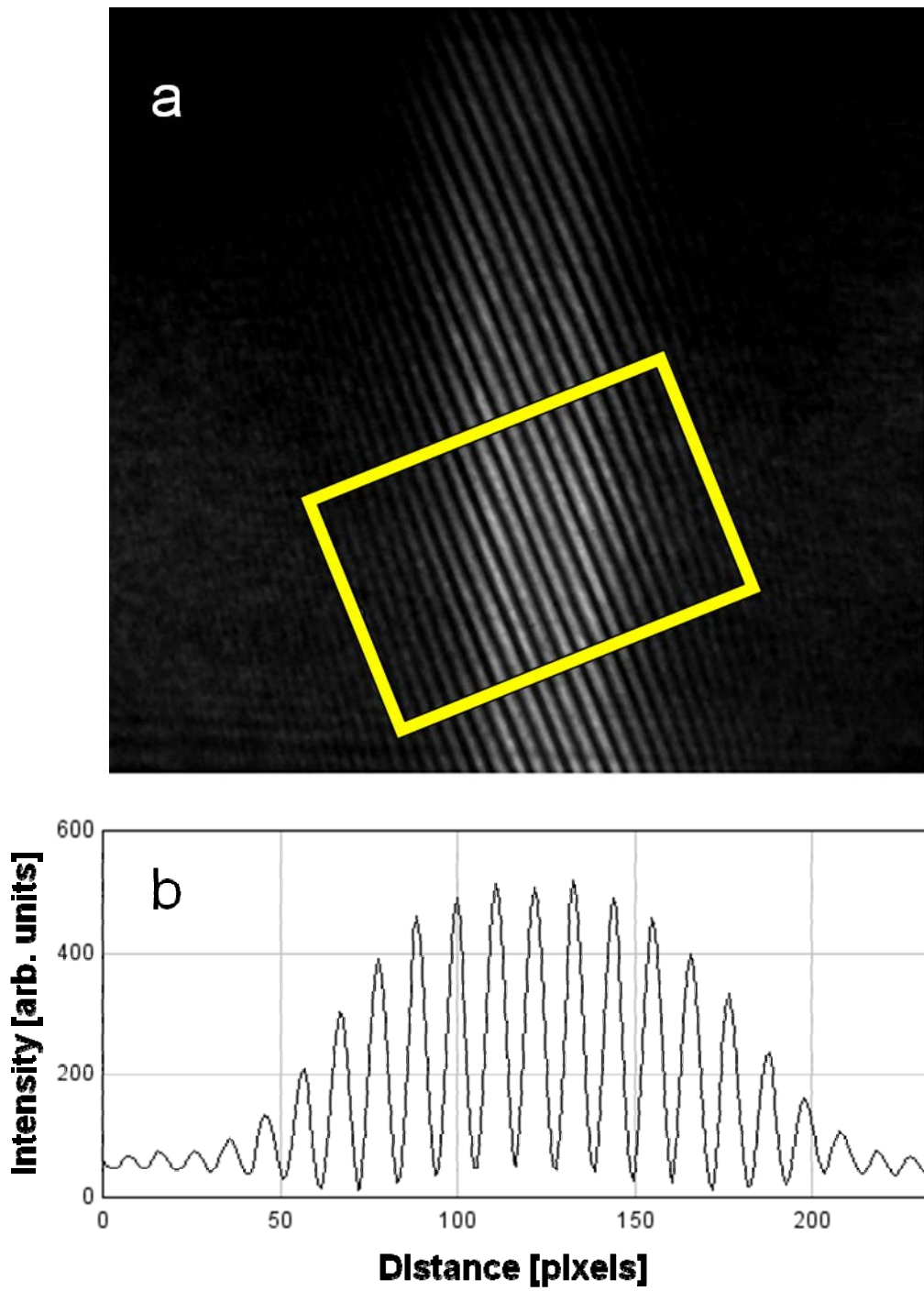


Figure 3

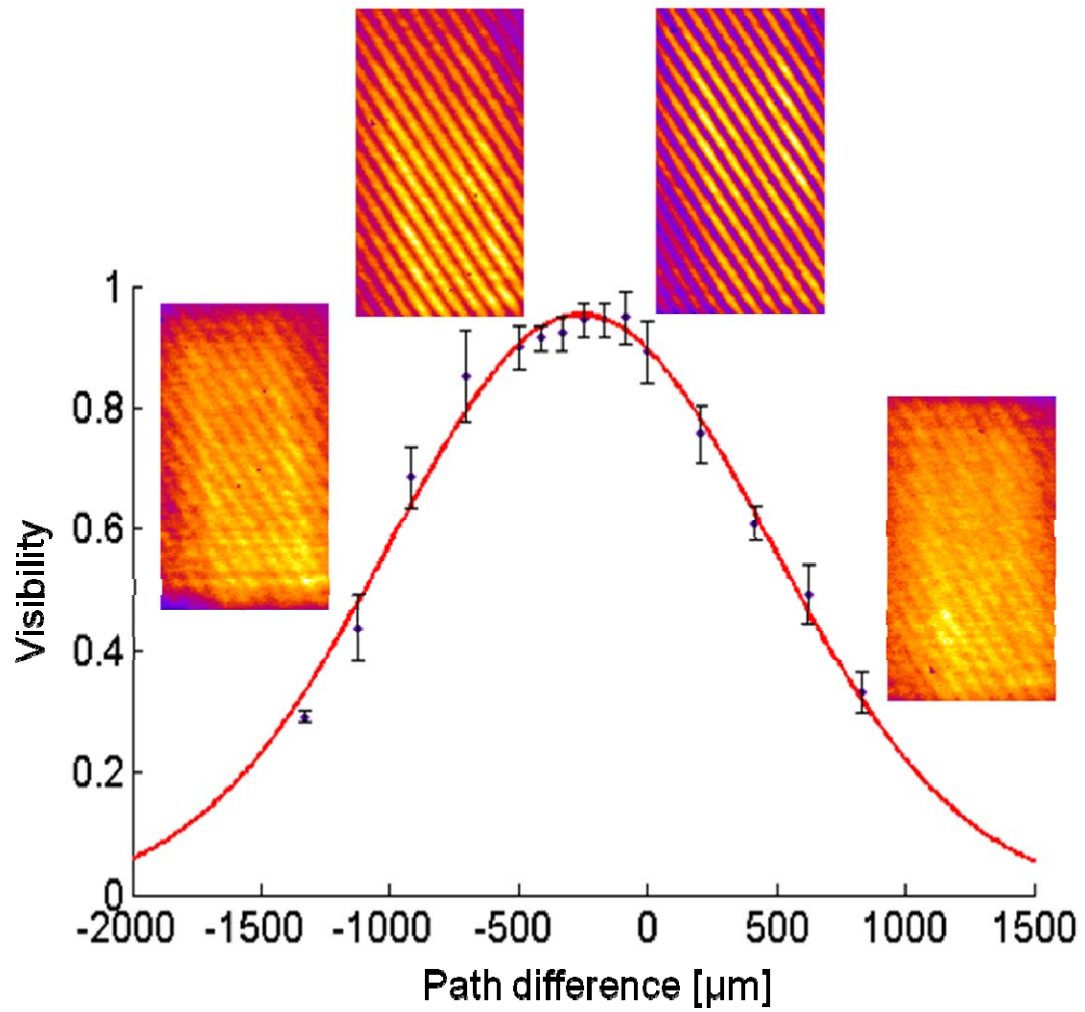
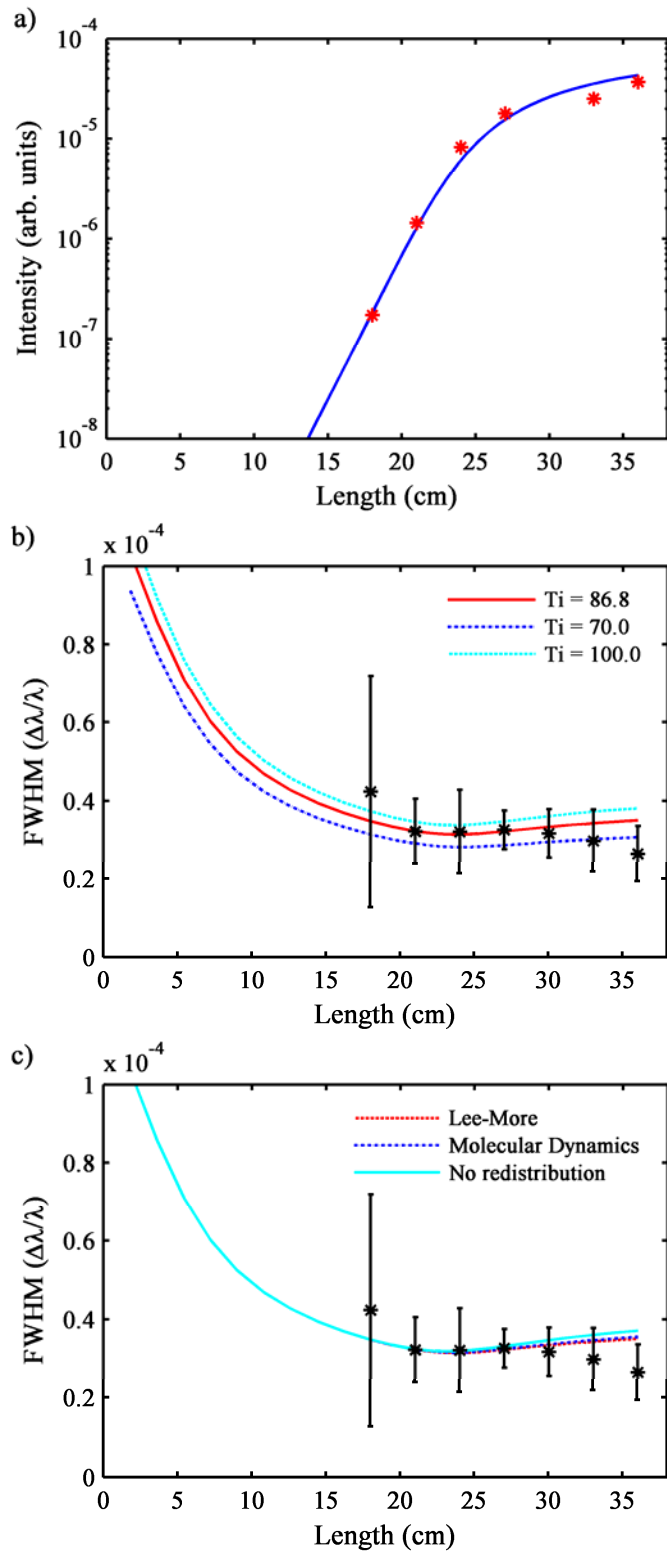


Figure 4



References

1. J.J. Rocca, V.N. Shlyaptsev, F.G. Tomasel, O.D. Cortazar, D. Hartshorn, J.L.A. Chilla, *Phys. Rev. Lett.* **73**, 2192 (1994).
2. B.R. Benware, C.D. Macchietto, C.H. Moreno, and J.J. Rocca, *Phys. Rev. Lett.* **81**, 5804 (1998).
3. C.D. Macchietto, B.R. Benware, J.J. Rocca, *Opt. Lett.* **24**, 1115 (1999).
4. J. Filevich, K. Kanizay, M.C. Marconi, J.L.A. Chilla, J.J. Rocca, *Opt. Lett.* **25**, 356 (2000).
5. C.A. Brewer, F. Brizuela, P. Wachulak, D.H. Martz, W. Chao, E.H. Anderson, D.T. Attwood, A.V. Vinogradov, I.A. Artyukov, A.G. Ponomareko, V.V. Kondratenko, M.C. Marconi, J.J. Rocca, C.S. Menoni, *Opt. Lett.* **33**, 518 (2008).
6. F. Brizuela, G. Vaschenko, C. Brewer, M. Grisham, C.S. Menoni, M.C. Marconi, J.J. Rocca, W. Chao, J.A. Liddle, E.H. Anderson, D.T. Attwood, A.V. Vinogradov, I.A. Artiukov, Y.P. Pershyn, and V.V. Kondratenko, *Opt. Express* **13**, 3983 (2005).
7. P.W. Wachulak, M.C. Marconi, R.A. Bartels, C.S. Menoni, J.J. Rocca, *J. Opt. Soc. Am. B* **25**, 1811 (2008).
8. P.W. Wachulak, M.G. Capeluto, M.C. Marconi, C.S. Menoni, J.J. Rocca, *Opt. Express* **15**, 3465 (2007).
9. L. Ottaviano, F. Bussolotti, S. Piperno, M. Rinaldi, S. Santucci, F. Flora, L. Mezi, P. Dunne, J. Kaiser, A. Reale, A. Ritucci, P. Zuppella, *Plasma Sources Sci. T.* **17**, 024019, (2008).
10. G. Vaschenko, A.G. Etxarri, C.S. Menoni, J.J. Rocca, O. Hemberg, S. Bloom, W. Chao, E.H. Anderson, D. T. Attwood, Y. Lu, and B. Parkinson, *Opt. Lett.* **31**, 3615 (2006).
11. L. Juha, M. Bittner, D. Chvostova, J. Krasa, Z. Otcenasek, A.R. Präg, J. Ullschmied, Z. Pientka, J. Krzywinski, J.B. Pelka, A. Wawro, M.E. Grisham, G. Vaschenko, C.S. Menoni, and J.J. Rocca, *Appl. Phys. Lett.* **86**, 034109 (2005).

12. S. Heinbuch, F. Dong, J.J. Rocca E.R. Bernstein, *J. of Chem. Phys.* **126**, 244301 (2007).
13. I.A. Artioukov, B.R. Benware, J.J. Rocca, M. Forsythe, Yu.A. Uspenskii, and A.V. Vinogradov, *IEEE J. Sel. Top. Quant.* **5**, 1495 (1999).
14. J.J. Rocca, D.P. Clark, J.L.A. Chilla, and V.N. Shlyaptsev, *Phys. Rev. Lett.* **77**, 1476 (1996).
15. A. Ben-Kish, M. Shuker, N.A. Nemirovsky, A. Fisher, A.Ron, J.L Schwob, *Phys. Rev. Lett.*, **87**, 015002, (2001)
16. G. Tomassetti, A. Ritucci, A. Reale, L. Palladino, L. Reale, S.V. Kuhklevski, F. Flora, L. Mezi, A. Faenov, T. Pikuz, A. Gaudieri, *Opt. Commun.*, **231**, 403, (2004)
17. S. Heinbuch, M. Grisham, D. Martz, J.J. Rocca, *Opt. Express* **13**, 4050 (2005).
18. S. Le Pape, Ph. Zeitoun, M. Idir, P. Dhez, J.J. Rocca, M. François, *Phys. Rev. Lett.* **88**, 183901 (2002).
19. M.C. Marconi, J.L.A. Chilla, C.H. Moreno, B.R. Benware, J.J. Rocca, *Phys. Rev. Lett.* **79**, 2799 (1997).
20. Y. Liu, M. Seminario, F.G. Tomasel, C. Chang, J.J. Rocca, and D.T. Attwood, *Phys. Rev. A* **63**, 033802 (2001).
21. J. A. Koch, B.J. MacGowan, L.B. Da Silva, D.L. Matthews, J.H Underwood, P.W Batson, R.W. Lee, R.A. London and S. Mrowka, 4th International Colloquium on X-Ray Lasers. Williamsburg, VA, (1994). X-RAY LASERS 1994 – Fourth International Colloquium Book Series: AIP Conference Proceedings. Issue: 332, pp 574-578, (1994).
22. J. A. Koch et al. *Phys. Rev. A*, **50**, 1877, (1994)
23. F. Tissandier, S. Sebban, M. Ribière, J. Gaautier, Ph. Zeitoun, G. Lambert, A. Barszczak Sardinha, J.-Ph Goddet, F. Burgy, T. Lefrou, C. Valentin, A. Rouse, O. Guilbaud, A. Klisnick, J. Nejd, T. Mocek, G. Maynard, *Phys. Rev. A* **81**, 063833, (2010)

24. R.F. Smith, J. Dunn, R. Hunter, J. Nilsen, S. Hubert, S. Jaquemot, C. Remond, R. Marmoret, M. Fajardo, P. Zeitoun, L. Vanbostal, C.L.S. Lewis, M.F. Ravet, F. Delmotte. *Opt. Lett.* **28**, 2261, (2003)
25. O. Guilbaud, A. Klisnick, D. Joyeux, D. Benredjem, K. Cassou, S. Kazamias, D. Ros, D. Phalippou G. Jamelot, *Eur. Phys. Journal D* **125**, (2006)
26. L.M.Meng, D. Alessi, O. Guilbaud, Y. Wang, M.Berrill, B.M. Luther, S.R. Domingue, D.H. Martz, D. Joyeux, S. De Rossi, J.J. Rocca, A. Klisnick, *Opt. Express* **19**, 12087, (2011)
27. A. Klisnick, O. Guilbaud, D. Ros, K. Cassou, S. Kazamias, G. Jamelot, J. C. Lagron, D. Joyeux, D. Phalippou, Y. Lechantre, M. Edwards, P. Mistry, G.J. Tallents, *J. Quant. Spectrosc. Ra.* **99**, 370 (2006).
28. R. London, *Phys. Fluids* **31**, 184, (1988).
29. J.L.A Chilla, J.J. Rocca, *J. of the Opt. Soc. of America B* **13**, 2841 (1996).
30. G.J. Pert. *Phys. Rev. A* **50**, 4412, (1994).
31. Y.T. Lee and R.M. More, *Phys. of Fluids* **27**, 1273, (1984).
32. B Talin, E Dufour, A Calisti, M A Gigosos, M A Gonzalez, T del Rio Gaztelurrutia and J W Dufty, *J. Phys. A: Math. Gen.* **36**, 6049 (2003)
33. S. Sebban, T. Mocek, D. Ros, L. Upcraft, Ph. Balcou, R. Haroutunian, G. Grillon, B. Rus, A. Klisnick, A. Carillon, G. Jamelot, C. Valentin, A. Rousse, J. P. Rousseau, L. Notebaert, M. Pittman, and D. Hulin, *Phys. Rev. Lett.* **25**, 253901, (2002)
34. A. Isoyan, F. Jiang, Y.C. Cheng, P. Wachulak, L. Urbanski, J. Rocca, C. Menoni, M.C. Marconi, F. Cerrina, *J. of Vac. Sc. and Techno.* **B27**, 2931, (2009).